



Effect of initial void ratio on the tensile strength of unsaturated silty soils

You Gao¹ · Ze Li¹ · Wenjie Cui² · De'an Sun³ · Haihao Yu⁴

Received: 15 March 2022 / Accepted: 14 January 2023 / Published online: 3 February 2023
© The Author(s), under exclusive licence to Springer-Verlag GmbH Germany, part of Springer Nature 2023

Abstract

The tensile strength of unsaturated soils is a fundamental property in various geotechnical designs. Reliable estimation of the tensile strength of unsaturated soils, in particular fine-grained soils, is required in both theoretical research and engineering practice. Although several tensile strength models have been proposed in the literature, an overestimation may occur over a wide suction range, when applying them in the modelling of tensile strength of fine-grained soils. In this paper, the tensile strength of an unsaturated lean clay has been measured over a wide range of void ratio and water content by employing the Brazilian tensile strength test. A critical degree of saturation can be observed for specimens with different void ratios, at which the soil tensile strength reaches the peak. In addition, a predictive tensile strength model considering the effect of initial void ratio has been subsequently proposed for both coarse-grained and fine-grained unsaturated soils based on the interaction mechanisms between the adsorptive and capillary soil water. Finally, the proposed model has been demonstrated to be capable of modelling the tensile strength characteristic curve of various soil types ranging from clean sands to silty and clayey soils.

Keywords Initial void ratio · Soil water characteristic curve · Tensile strength · Unsaturated soil

1 Introduction

The tensile strength of soils plays an important role in the initiation of cracks in soils during drying process. Most engineering problems involving structure cracks, in particular the top area of many slopes and highway pavements, are associated with tensile strength of soils [4]. The

existence of tensile cracks can significantly affect the hydro-mechanical properties of soils, such as stiffness, cohesion, soil water retention behaviour, and permeability [40, 41], especially for the fine-grained soils, which is susceptible to environmental changes, such as soil moisture, temperature, and relative humidity [22]. Therefore, tensile strength and tensile strength testing of soils have received increasing attention in recent decades.

The tensile strength of unsaturated soils can be measured by either a direct or an indirect approach in the laboratory testing. For the direct approach, the tensile strength is usually determined by uniaxial tensile tests. Lu et al. [33] investigated the tensile strength of sands over a full range of degree of saturation by a simple uniaxial tensile test. Tang et al. [39] developed a simple direct tensile apparatus to determine the tensile strength of compacted clayey soils over a wide range of water contents. Cai et al. [8] designed a wedge-shaped specimen mould to measure the tensile strength of unsaturated fine sands. Direct methods always require relatively complex specimen geometries to ensure the location of the failure plane, such as “8”-shaped specimens [38] and wedge-

✉ Wenjie Cui
wcui21@buaa.edu.cn

✉ De'an Sun
sundean@shu.edu.cn

¹ School of Civil and Environmental Engineering, Ningbo University, 818 Fenghua Road, Ningbo 315211, China

² School of Transportation Science and Engineering, Beihang University, 37 Xueyuan Road, Haidian District, Beijing 100191, China

³ Department of Civil Engineering, Shanghai University, 99 Shangda Road, Shanghai 200444, China

⁴ Laboratory of Geomechanics and Geotechnical Engineering, Guilin University of Technology, 12 Jian Gan Road, Guilin 541004, China

shaped specimens [8, 42]. The major drawback of the direct methods is that relative sliding between rigid fixtures and specimens may result in the destruction of the specimen ends and hence cause inaccurate results [26].

The indirect methods include the Brazilian tensile strength test [2, 5, 7], unconfined penetration test [22, 27], and bending test [34], in which the tensile stress is indirectly determined by dividing the applied force over the cross-sectional area of the failure surface. Among the above indirect testing methods, the Brazilian tensile strength (BTS) test is the most frequently used one, due to its advantages in the relatively simple testing procedure, and the specimen and testing equipment which is the same as that for the compression tests [11]. In addition, the tensile strength of the failure surface in the BTS test is uniform, which ensures the accuracy of the measured results.

In order to account for the effect of matric suction on the tensile strength of unsaturated soils, a number of models have been proposed in recent decades. Kim and Sture [23] proposed a model for describing the tensile strength of unsaturated sands in funicular and capillary regions. Lu et al. [31] presented a tensile strength model that is capable of predicting the tensile strength of unsaturated sands. Yin and Vanapalli [45] established a semi-empirical model for predicting the tensile strength of unsaturated cohesionless soils. Zhai et al. [46] estimated the tensile strength of unsaturated sandy soils by adopting the concept of pore-size distribution. The above tensile strength models were developed based on the regression analyses of experimental data from either direct or indirect tests for coarse-grained soils. An overestimation may occur, when applying them in the modelling of tensile strength of fine-grained soils, especially in the medium and high suction ranges. To overcome this problem, Varsei et al. [43] suggested that the effective stress coefficient χ in the shear strength criteria should be replaced by $(S_r)^k$, where k is a fitting parameter and $k \geq 1$. Salimi et al. [37] proposed a general tensile strength model based on the concept of capillary and suction stress. However, general tensile strength models that can reasonably predict the tensile strength of various types of unsaturated soils are limited in the literature. Moreover, the effect of the initial void ratio on the tensile strength of unsaturated soils is notable over a wide suction range in the experimental tests, especially for fine-grained soils [18]. Therefore, it is necessary to investigate the tensile strength of unsaturated soils with different initial void ratios over a wide suction range.

The main objective of this study is to investigate the tensile strength behaviour of various soil types with different initial void ratios and water contents. Firstly, a series of experimental tests were performed over a wide water content range and a comprehensive analysis of the features

of the tensile strength behaviour was carried out. Subsequently, a model was proposed based on the modified soil water characteristic curve (SWCC) equation to describe the tensile strength of various soil types with different initial void ratios. Finally, the proposed model was verified by comparing against experimental data obtained in this study and that reported in the literature.

2 Material

The soil specimen used in this study is composed of an approximately 13% clay fraction and an approximately 84% silt fraction. It has a liquid limit of 28.7%, a plastic limit of 18.9, a maximum dry density of 1.81 Mg/m³ and a specific gravity of 2.70. The measured physical and mechanical properties are shown in Table 1. According to the unified soil classification system [1], the soil is classified as lean clay (CL).

3 Testing methods

All specimens used in this study were prepared by static compaction in a constant volume compaction mould with an inside diameter of 61.8 mm and a height of 20 mm. To prepare these compacted specimens, the soil sample was first air-dried and crushed. The completely dry soil powder was then passed through a 2-mm standard sieve before being mixed with distilled water to achieve the required water content. The mixtures were sealed and stored for 24 h. Finally, the specimens were completed after compaction in a mould with a constant volume.

The BTS test has been employed to measure the tensile strength with different initial states. Figure 1 shows the displacement-controlled triaxial instrument for measuring

Table 1 Physical and mechanical property indexes of test soil

| Soil properties | Value |
|--|-------|
| Specific gravity | 2.70 |
| Liquid limit (%) | 28.7 |
| Plastic limit (%) | 18.9 |
| Plastic index | 9.77 |
| Optimum water content (%) | 15.71 |
| Maximum dry density (Mg/m ³) | 1.81 |
| Silt content (%) | 84 |
| Clay content (%) | 13 |
| Unified soil classification system | CL |
| Cohesion (kPa) | 5 |
| Effective internal friction angle (°) | 25 |

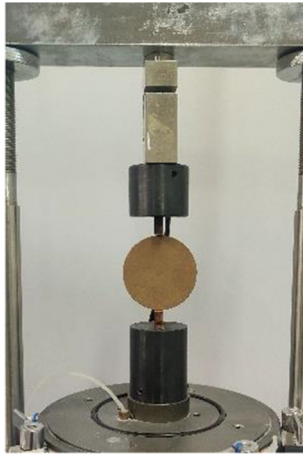


Fig. 1 Apparatus for Brazilian tensile strength test

the tensile strength of unsaturated specimens, which is equipped with a load sensor and a displacement sensor. As shown in Fig. 1, the compacted specimen was placed radially between two rigid loading blocks. A loading rate of 0.1 mm/min was selected for the BTS test. The tensile strength of the specimen can be determined as follows:

$$\sigma_t = \frac{2P}{\pi dt} \quad (1)$$

where σ_t is the tensile strength, kPa; P is the axial load, kN; d is the diameter, m; and t is the thickness of the specimen, m.

To investigate the effect of the initial void ratio and water content on the tensile strength behaviour, the compacted specimens with different initial void ratios and water contents were prepared, as listed in Table 2.

4 Test results and discussions

Figure 2 illustrates the evolution of measured tensile strength characteristic curves (TSCC) with water content (w) and degree of saturation (S_r) at initial void ratios of approximately 0.80, 0.69, and 0.59, respectively. All curves exhibit similar features with a clearly observed peak tensile strength, indicating that the tensile strength depends significantly on w or S_r at a given void ratio. When the specimen was in the relatively dry status, the tensile strength increased with increasing water content or degree of saturation. For specimens with different void ratios, a peak value of the tensile strength was observed at the same critical degree of saturation, S_{rc} , of approximately 26%. Further wetting the specimen leads to the decreasing in the tensile strength. However, the decreasing rate becomes more gradual when the water content is higher than the optimum water content, w_{op} , indicating that the tensile

Table 2 Initial states of all specimens

| Test no. | Initial water content (%) | Initial void ratio | Initial degree of saturation (%) |
|----------|---------------------------|--------------------|----------------------------------|
| 1 | 4.1 | 0.59 | 18.76 |
| 2 | 4.1 | 0.69 | 16.04 |
| 3 | 5.9 | 0.59 | 27.00 |
| 4 | 5.9 | 0.69 | 23.09 |
| 5 | 5.9 | 0.80 | 19.91 |
| 6 | 8.2 | 0.59 | 37.53 |
| 7 | 8.2 | 0.69 | 32.09 |
| 8 | 8.2 | 0.80 | 27.68 |
| 9 | 9.8 | 0.59 | 44.85 |
| 10 | 9.8 | 0.69 | 38.35 |
| 11 | 9.8 | 0.80 | 33.08 |
| 12 | 11.8 | 0.59 | 54.00 |
| 13 | 11.8 | 0.69 | 46.17 |
| 14 | 11.8 | 0.80 | 39.83 |
| 15 | 14.0 | 0.59 | 64.07 |
| 16 | 14.0 | 0.69 | 54.78 |
| 17 | 14.0 | 0.80 | 47.25 |
| 18 | 15.9 | 0.59 | 72.76 |
| 19 | 15.9 | 0.69 | 62.22 |
| 20 | 15.9 | 0.80 | 53.66 |
| 21 | 18.2 | 0.59 | 83.29 |
| 22 | 18.2 | 0.69 | 71.22 |
| 23 | 18.2 | 0.80 | 61.43 |

strength is not sensitive to the variation in the water content when the water content is sufficiently high. In addition, decreasing the initial void ratio leads to a rise in the tensile strength at a given water content.

Within a low degree of saturation range ($S_r < S_{rc}$), most of the water is trapped in intra-aggregate pores. The compacted specimens at this stage are located in the region of intra-aggregate governing suction [36, 10, 39]. Although the soil suction is high, it contributes less to the tensile strength, that is, the contribution of suction to the tensile strength will decrease with decreasing degree of saturation ($S_r < S_{rc}$), as shown in Fig. 2b. When the degree of saturation is higher than the critical value ($S_r > S_{rc}$), a decreasing trend in tensile strength is observed. An increasing number of water-bridges disappear at the contact points of the inter-aggregate with increasing the degree of saturation. The contribution of suction to the tensile strength will decrease with increasing the degree of saturation ($S_r > S_{rc}$).

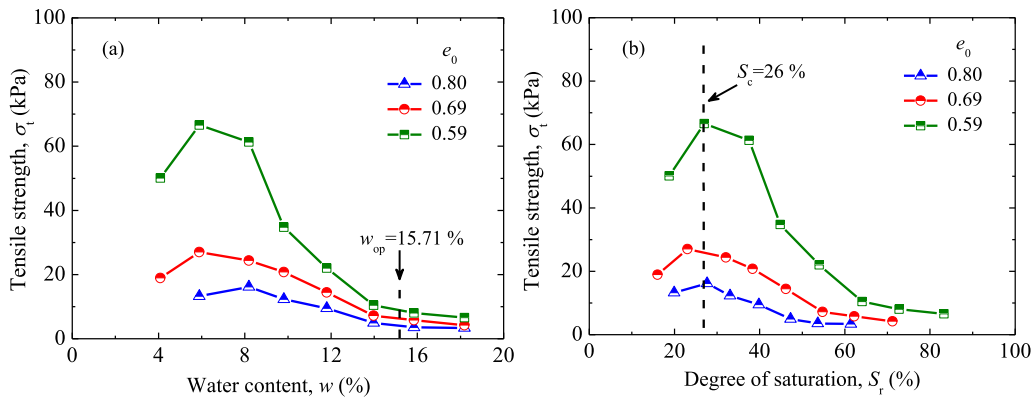


Fig. 2 Measured variation in tensile strength at different initial void ratios with a water content and b degree of saturation

5 Modified SWCC model for adsorption and capillarity

As demonstrated by the experimental results shown above, the tensile strength of unsaturated soils depends on the associated water content and initial void ratio. To adequately simulate this behaviour, a modified SWCC model is required which is not only able to account for the effect of void ratio on the water retention evolution, but also capable of producing accurate prediction over a wide suction range. Therefore, a modified SWCC model is developed in this section.

In recent years, it has been acknowledged that two types of pore water exist in unsaturated soils: capillary water and adsorbed water [3, 23, 28, 49]. As a result, the water content of unsaturated soils can be written as

$$w = w_a + w_c \tag{2}$$

where w is the total water content, %; w_a is the adsorption water content, %; and w_c is the capillarity water content, %.

To account for the adsorption water content, Revil and Lu [35] proposed a function associated with the relative humidity-based Kelvin’s law [12] which can be expressed as

$$w_a = w_{am} \left[\exp \left(- \frac{s\omega_v}{\rho_w RT} \right) \right]^{1/M} \tag{3}$$

where w_{am} is the maximum adsorption water content, %, and M is the adsorption strength, s is the suction, kPa, ω_v is the molecular mass of water vapour assumed as a constant of 18.016 g/mol, R is the universal gas constant (i.e. 8.314 J/mol K), ρ_w is the density of water, Mg/m³, and T is the absolute temperature, K.

In addition, the quantity of $\rho_w RT/\omega_v$ is a constant of 137,000 kPa at room temperature (25 °C) in Eq. (3). This indicates that the suction reaches its maximum suction value at zero water content is 137000 kPa. However, experimental data have shown that the suction of a soil

reaches its maximum suction value at zero water content, which can be much higher than 137,000 kPa [13, 30, 36]. To simulate the high suction value closed to zero water content, a correction factor $C(s)$ proposed by Fredlund and Xing (1994) is given by

$$C(s) = 1 - \frac{\ln(1 + s/s_r)}{\ln(1 + s_m/s_r)} \tag{4}$$

where s_r is the residual suction, kPa. s_m is the maximum suction, kPa. Lu and Khorshidi [30] reported that the maximum suction varies from 475 to 1180 MPa and depends on the soil mineralogy. It indicated that the highest total suction in the SWCC models should not set the upper bound to a fixed value.

Substituting Eq. (4) into Eq. (3), the adsorption water content equation can be expressed as

$$w_a = w_{am} C(s) \left[\exp \left(- \frac{s\omega_v}{\rho_w RT} \right) \right]^{1/M} \tag{5}$$

Incorporating the adsorption degree of saturation S_{ra} , which is equal to $w_a G_s / e_a$ (G_s is specific gravity, and e_a is the void ratio), into Eq. (5) can be further expressed as follows:

$$S_{ra} = \frac{w_{am} G_s}{e_a} C(s) \left[\exp \left(- \frac{s\omega_v}{\rho_w RT} \right) \right]^{1/M} \tag{6}$$

The change of the adsorption degree of saturation is mainly dependent on soil types (i.e. mineralogical composition) [30, 36]. In the high suction range, the variation of the adsorption degree of saturation with suction is highlighted, but e_a does not change significantly with increasing suction. That indicated that the e_a had negligible influence on the adsorption degree of saturation at a given initial state. In addition, the value of e_a is difficult to be determined over a wide suction range. For simplicity, it is assumed that e_0 is proportional to the e_a ($e_0 = \beta e_a$, β is a material parameter which is larger than 1). Substituting

$e_0 = \beta e_a$ into Eq. (6), the adsorption degree of saturation can be further derived as

$$S_{ra} = \frac{\beta w_{am} G_s}{e_0} C(s) \left[\exp\left(-\frac{s\omega_v}{\rho_w RT}\right) \right]^{1/M} \tag{7}$$

Equivalently, Eq. (7) can be rewritten as

$$S_{ra} = \frac{w_m}{e_0} C(s) \left[\exp\left(-\frac{s\omega_v}{\rho_w RT}\right) \right]^{1/M} \tag{8}$$

where w_m is a material parameter expressed as $w_m = \beta w_{am} G_s$. The parameter w_m can be determined by fitting the experimental data of SWCCs.

Following the theory proposed by Khlosi et al. [20], the capillary water content (i.e. capillary water characteristic curve) can be expressed as

$$w_c = (w_s - w_a) f(s) \tag{9}$$

where w_s is the saturated water content, %, and $f(s)$ is the capillary component function. Replacing $f(s)$ by the formulation proposed by Fredlund and Xing [13], Eq. (9) can be further expressed as

$$w_c = (w_s - w_a) C_c(s) \left\{ \ln \left[e + \left(\frac{s}{a} \right)^n \right] \right\}^{-m} \tag{10}$$

where a , m and n are the fitting parameters, e is the natural number, $e = 2.71828$. $C_c(s)$ is a correction factor for capillary water, expressed as $C_c(s) = 1 - \ln(1 + s/s_r) / \ln(1 + s_{cm}/s_r)$, in which s_{cm} is the upper bound of capillary suction(kPa). When $C_c(s)$ equals to $C(s)$, the upper bound of the capillary suction becomes the maximum suction and Eq. (10) may overestimate capillary water content in some soils. To overcome this shortcoming, it is assumed that the upper bound of capillary suction is equal to the residual suction, i.e. $C_c(s) = 1 - \ln(1 + s/s_r) / \ln(2)$.

Similarly, the capillary degree of saturation S_{rc} can be given as:

$$S_{rc} = (1 - S_{ra}) C_c(s) \left\{ \ln \left[e + \left(\frac{s}{a} \right)^n \right] \right\}^{-m} \tag{11}$$

By combining Eqs. (8) and (11), a SWCC model accounting for both adsorption and capillarity water can be written as

$$S_r = S_{rc} + S_{ra} = (1 - S_{ra}) C_c(s) \left\{ \ln \left[e + \left(\frac{s}{a} \right)^n \right] \right\}^{-m} + \frac{w_m}{e_0} C(s) \left[\exp\left(-\frac{s\omega_v}{\rho_w RT}\right) \right]^{1/M} \tag{12}$$

Equation (12) involves seven physical parameters in total, where three, i.e. a , n , and m , account for the effect of capillary water, while two, i.e. w_m and M , are employed to model the effect of adsorption water. The remaining two parameters s_r and s_m represent the residual suction and the maximum suction, respectively.

The initial void ratio is a key factor affecting the hydraulic properties of unsaturated soils. Many studies [14–16] suggested that the shifting of the SWCC due to the void ratio can be modelled by introducing a term of $(e_0)^b$ into the suction s , where b is a fitting parameter. Following a similar approach, Eq. (12) can be further expressed as

$$S_r(s, e_0) = (1 - S_{ra}) C_c(s) \left\{ \ln \left[e + \left(\frac{e_0^b s}{a} \right)^n \right] \right\}^{-m} + \frac{w_m}{e_0} C(s) \left[\exp\left(-\frac{e_0^b s \omega_v}{\rho_w RT}\right) \right]^{1/M} \tag{13a}$$

As absorbed water does not exist in coarse-grained soils, especially for sandy soils [18], the adsorption degree of saturation can be assumed to be zero for coarse-grained soils and the upper bound of capillary suction is equal to the residual suction, i.e. $C(s) = C_c(s)$. Therefore, the void ratio-dependent equation for coarse-grained soils with different initial void ratios can be simplified as

$$S_r(s, e_0) = S_{rc}(s, e_0) = C(s) \left\{ \ln \left[e + \left(\frac{e_0^b s}{a} \right)^n \right] \right\}^{-m} \tag{13b}$$

The proposed SWCC model (Eq. 13) was validated against existing experimental results of four different types of soils, namely silty sand, clayey silty sand, silty clay, and expansive soil [25, 36, 19, 48]. The basic physical properties and initial void ratio of four selected soils are listed in Table 3. Figure 3 shows the comparison between the measured SWCCs of four selected soils with different void ratios and the corresponding predictions by the proposed model with the parameters listed in Table 4. The good agreement between the experimental and predicted results

Table 3 Properties of four different types of soils

| Soil type | Specific gravity | Liquid limit (%) | Plastic limit (%) | Initial void ratio | | | | USCS | |
|-------------------|------------------|------------------|-------------------|--------------------|-------|-------|------|------|-------|
| Silty sand | 2.65 | N.G | N.G | 0.56 | 0.51 | 0.48 | 0.45 | SM | |
| Clayey silty sand | 2.65 | 25 | 14.5 | 0.36 | 0.47 | 0.61 | 0.77 | 0.96 | SC-CL |
| Silty clay | 2.73 | 35.5 | 16.8 | 0.514 | 0.474 | 0.444 | | | CL |
| Expansive Soil | 2.74 | 38.8 | 17.2 | 1.19 | 1.03 | 0.83 | | | CL |

N.G. not given, USCS Unified Soil Classification System

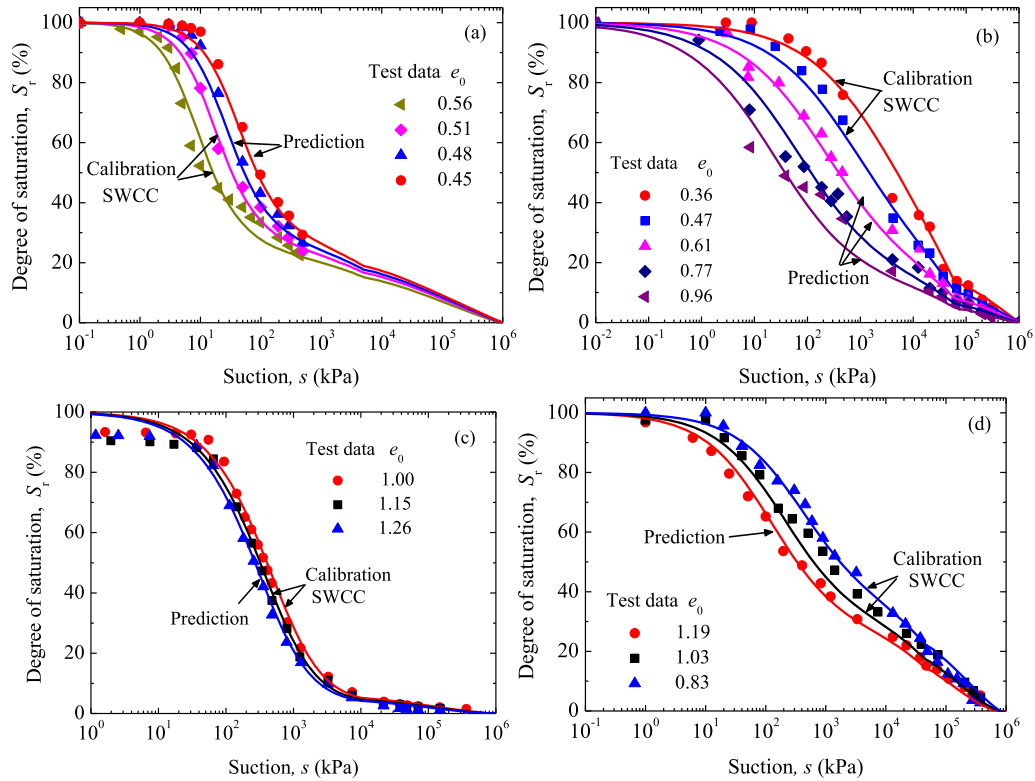


Fig. 3 Comparison of measured and predicted SWCCs of **a** silty sand, **b** clayey silty sand, **c** silty clay, and **d** expansive soil

Table 4 Parameters of proposed SWCC model for different types of soils with different void ratios

| Soil type | <i>b</i> | <i>w_{am}</i> (%) | <i>M</i> | <i>a</i> | <i>m</i> | <i>n</i> | <i>s_r</i> (MPa) | <i>s_m</i> (MPa) |
|-------------------|----------|---------------------------|----------|----------|----------|----------|----------------------------|----------------------------|
| Silty sand | 7.2 | 3.7 | 1.0 | 0.1 | 1.55 | 1.35 | 5 | 1000 |
| Clayey silty sand | 4.8 | 2.5 | 8.0 | 26 | 2.15 | 0.52 | 60 | 1000 |
| Silty clay | 2.0 | 2.5 | 7.5 | 980 | 4.10 | 0.85 | 10 | 1000 |
| Expansive soil | 3.3 | 9.0 | 6.0 | 150 | 1.85 | 0.75 | 45 | 800 |

demonstrates that the proposed SWCC model is capable of simulating the SWCCs of various types of soil as well as the influence of the void ratio on the SWCC.

6 Tensile strength characteristic curve (TSCC) model for adsorption and capillarity

In the past decades, a number of theoretical and empirical models have been developed to predict the tensile strength of soils [21, 31, 43, 44, 46]. In most models, the tensile strength is usually obtained based on Mohr–Coulomb’s

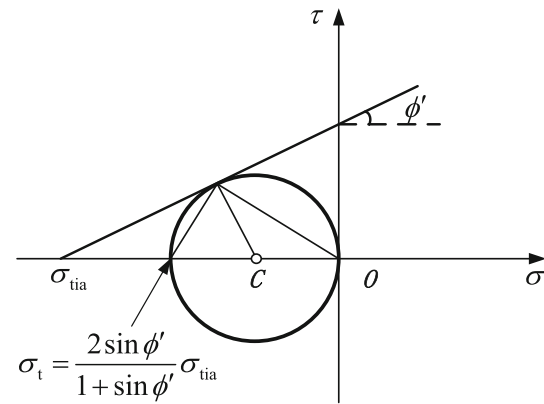


Fig. 4 Mohr–Coulomb’s criterion for uniaxial tensile strength (modified by Lu et al. 2009)

criterion, as shown in Fig. 4. The equation for the uniaxial tensile strength is given as

$$\sin \phi' = \frac{\sigma_t/2}{(\sigma_{tia} - \sigma_t/2)} = \frac{\sigma_t}{(2\sigma_{tia} - \sigma_t)} \tag{14}$$

where ϕ' is the effective internal friction angle; and σ_{tia} is the isotropic tensile strength.

The relationship between the isotropic tensile strength and uniaxial tensile strength can be obtained by rearranging Eq. (14) as

$$\sigma_t = \frac{2 \sin \phi'}{1 + \sin \phi'} \sigma_{tia} \quad (15)$$

$$\sigma_t = 2 \tan \phi' \tan \left(\frac{\pi}{4} - \frac{\phi'}{2} \right) \sigma_{tia} \quad (16)$$

The suction stress can be conceptualized as the isotropic tensile strength [31], given as

$$\sigma_{tia} = \sigma^s \quad (17)$$

where σ^s is suction stress. The suction stress can be decomposed into two water content-dependent components: adsorptive suction stress, σ_a^s , and capillary suction stress, σ_c^s , given as

$$\sigma^s = \sigma_a^s + \sigma_c^s \quad (18)$$

In the residual regime, the suction stress may diminish to zero for coarse-grained soil but could reach several hundred kPa for fine-grained soil due to van der Waals stress approaches a constant value [29, 32]. To account for the adsorption suction stress of fine-grained soil in the residual regime, Zhang and Lu [47] proposed an adsorption suction stress which can be expressed as

$$\sigma_a^s = f_a(S_r) \sigma_{dry}^s \quad (19)$$

where σ_{dry}^s is the suction stress at the over dry state, which is a soil property combining the effects of contact area and mineral properties on suction stress and independent of water content or matric suction. $f_a(S_r)$ is dimensionless scaling function, which reflects distribution of physico-chemical forces in terms of probability. By combining Eq. (13b), $f_a(S_r, e_0)$ can be given as

$$f_a(S_r, e_0) = \frac{1}{2} \left[1 - \operatorname{erf} \left(\beta \frac{S_r(s, e_0) - S_r^{\text{tran}}(s, e_0)}{S_r^{\text{tran}}(s, e_0)} \right) \right] \quad (20)$$

where β is a dimensionless parameter reflecting the strength of adsorptive suction stress and depends on soil types and soil fabrics, expansive clays have wider transition zones and much lower β values than nonexpansive clays. S_r^{tran} is the degree of saturation at which adsorption water regime transitions to capillary water regime. Zhang and Lu [47] suggested the ratio of S_r^{tran} to S_{ra}^{max} follows 1.55 closely. S_{ra}^{max} is the maximum adsorption saturation.

In many strength criteria for unsaturated soil, the degree of saturation or effective degree of saturation has been adopted as the effective stress coefficient. However, this may lead to a significant overestimation of the tensile strength of unsaturated soil in the capillary regime, especially for fine-grained soils. Varsei et al. [43] suggested that the effective stress coefficient in the shear strength criteria should be replaced by $(S_r)^k$. By considering the effect of the void ratio on the tensile strength, the capillary suction stress can be written as

$$\sigma_c^s = s[S_{rc}(s, e_0)]^k \quad (21)$$

For coarse-grained soils, $k = 1$ and $S_{ra} = 0$, as there is barely any adsorbed water in coarse-grained soils, while for fine-grained soils, $k > 1$ and $S_{ra} \neq 0$. Based on Eqs. (13), (18), (19) and (21), the uniaxial tensile strength can be given as

$$\sigma_t = 2 \tan \phi' \tan \left(\frac{\pi}{4} - \frac{\phi'}{2} \right) s S_r(s, e_0) \quad (22a)$$

for coarse - grained soil

$$\sigma_t = 2 \tan \phi' \tan \left(\frac{\pi}{4} - \frac{\phi'}{2} \right) \left[f_a(S_r, e_0) \sigma_{dry}^s + s[S_{rc}(s, e_0)]^k \right] \quad (22b)$$

for fine - grained soil

The tensile strength of different types of soils with different void ratios can be predicted using Eqs. (13a), (13b) and (22). The parameters of Eqs. (13a) and (13b) can be determined by fitting the two arbitrary SWCC. For fine-grained soils, the material parameter k and β can be calibrated by the measured tensile strength of the specimen with an arbitrary void ratio. For coarse-grained soils, the material parameter k is adopted as a constant of 1.

7 Model verification

7.1 Fine-grained soils

In the experimental study shown earlier, the drying SWCCs of test soil, i.e. lean clay, were measured at initial moulding void ratios of approximately 0.80, 0.69 and 0.59 using the filter paper method and vapour equilibrium method, as shown in Fig. 5. AWCC and CWCC represent the adsorption water characteristic curve and capillary water characteristic curve, respectively. SWCCs of test soil with different void ratios can be well simulated using Eq. (13a) with the parameters listed in Table 5.

Figure 6 shows the measured and predicted tensile strength of test soil with three void ratios ($e_0 = 0.80, 0.69$ and 0.59). The material parameter k in Eq. (22b) was set as 2.5, based on the calibration against the measured tensile strength of the specimen with an initial void ratio of 0.59. Then, the calibrated proposed model (i.e. Equation (13) and Eq. (22b)) was used to model the tensile strength curves at the other two void ratios, yielding a good agreement.

Experimental data of two residual clays, one from the Bukit Timah Granite (BTG) and the other from the Jurong Formation (JF) [7], have also been employed for model validation. The initial void ratios of compacted BTG residual clay specimens were 0.445, 0.486, 0.529, and

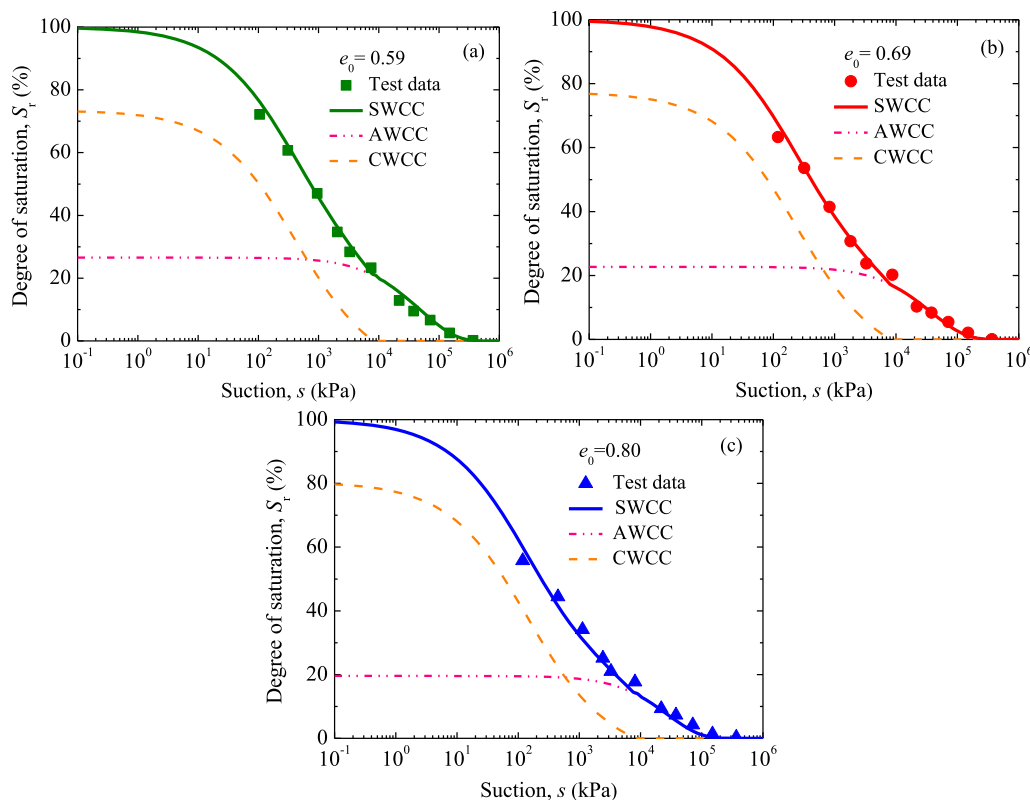


Fig. 5 Comparison of measured and predicted SWCCs of test soil at different initial void ratios with a $e_0 = 0.59$, b $e_0 = 0.69$ and c $e_0 = 0.80$

Table 5 Parameters of proposed model for fine-grained soils with different void ratios

| Soil name | b | w_{am} (%) | M | a | m | n | s_r (MPa) | s_m (MPa) | β |
|-------------------|------|--------------|------|------|------|------|-------------|-------------|---------|
| Test soil | 3.20 | 5.8 | 0.19 | 65 | 2.58 | 0.65 | 8 | 1000 | 3 |
| BTG residual clay | 1.60 | 5.2 | 0.20 | 2800 | 2.95 | 1.10 | 10 | 600 | 2 |
| JF residual clay | 0.88 | 5.1 | 0.45 | 2350 | 6.80 | 1.29 | 12 | 300 | 2 |

0.565, while the initial void ratios of the compacted JF residual clay specimens were 0.473, 0.549, and 0.594. The plastic limit of the BTG residual clay and JF residual clay was 31% and 24%, respectively. The effective internal friction angles of the BTG residual clay and JF residual clay under fully saturated conditions were 28 and 30°, respectively. The tensile strength of soil was determined by Brazilian tensile strength tests.

Figures 7 and 8 show the measured and fitted SWCCs of BTG residual clay and JF residual clay with different initial void ratios. The adopted model parameters for BTG residual clay and JF residual clay are listed in Table 5. A good agreement can be observed at different void ratios.

Figures 9 and 10 show the measured and predicted tensile strength of BTG residual clay and JF residual clay with different initial void ratios (i.e. $e_0 = 0.445$, 0.486, 0.529 and 0.565 for BTG residual clay, and $e_0 = 0.473$,

0.549, and 0.594 for JF residual clay). The material parameter k for the BTG and JF residual clays was set as 2.3, which were calibrated based on the measured tensile strength of specimens with initial void ratio of 0.445 (see Fig. 9a) and 0.473 (see Fig. 10a). The calibrated model was subsequently used to simulate the tensile strength curves at other void ratios. The good agreement between the measured data and model predictions demonstrates that the proposed model is capable of accurately capturing the tensile strength behaviour of two clays with different initial void ratios.

7.2 Coarse-grained soils

Figure 11 shows comparison between the measured and predicted SWCC and TSCC for Esperance sand with initial porosities of 0.4 and 0.45 (i.e. initial void ratios of 0.67 and

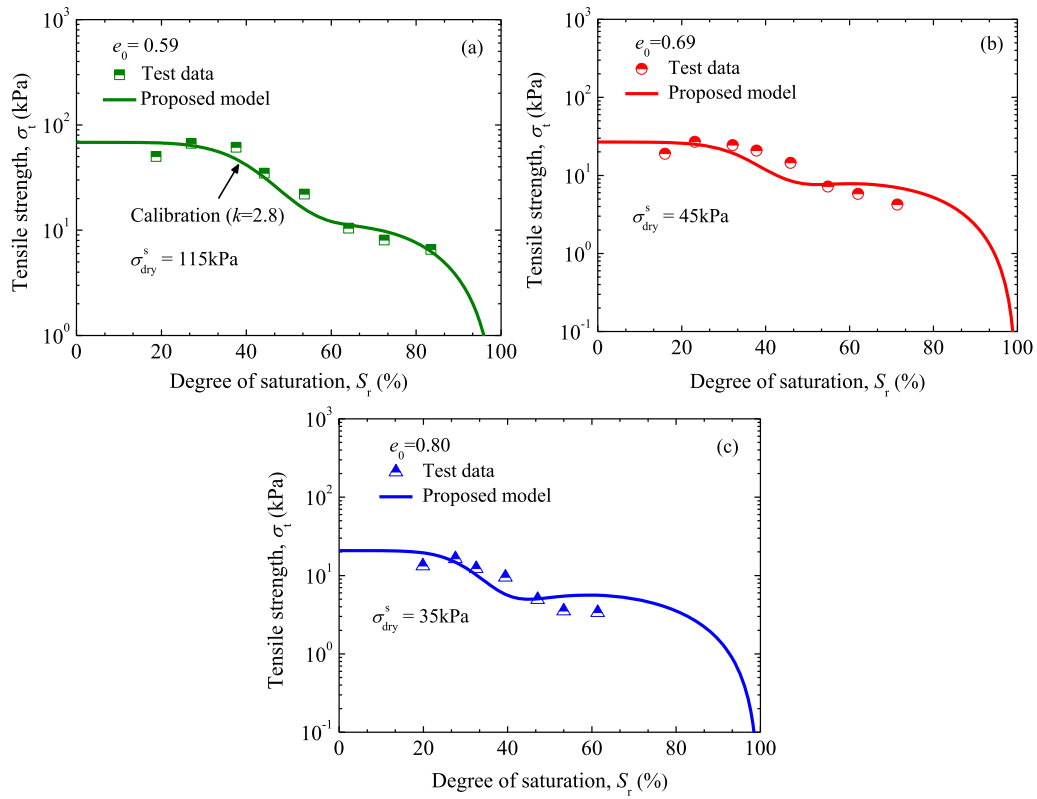


Fig. 6 Comparison in tensile strength of test soil between experimental data and model prediction at different initial void ratios with **a** $e_0 = 0.59$, **b** $e_0 = 0.69$ and **c** $e_0 = 0.60$

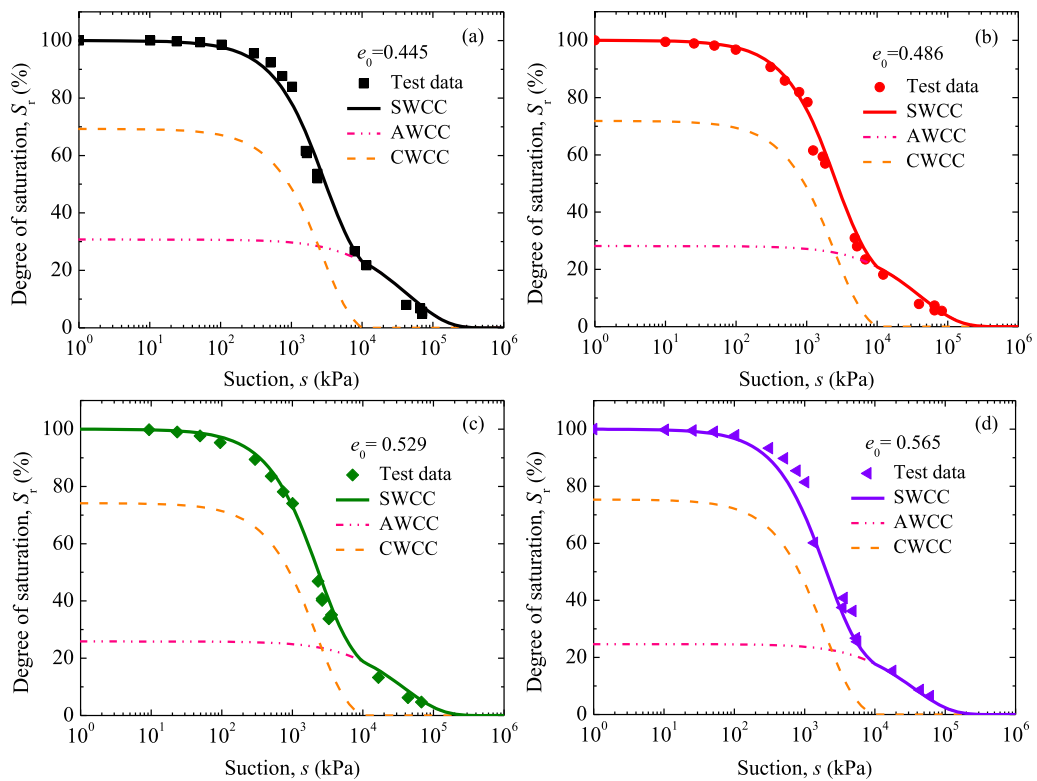


Fig. 7 Comparison of measured and fitted SWCCs of BTG residual clay with **a** $e_0 = 0.445$, **b** $e_0 = 0.486$, **c** $e_0 = 0.529$ and **d** $e_0 = 0.565$ (data from [7])

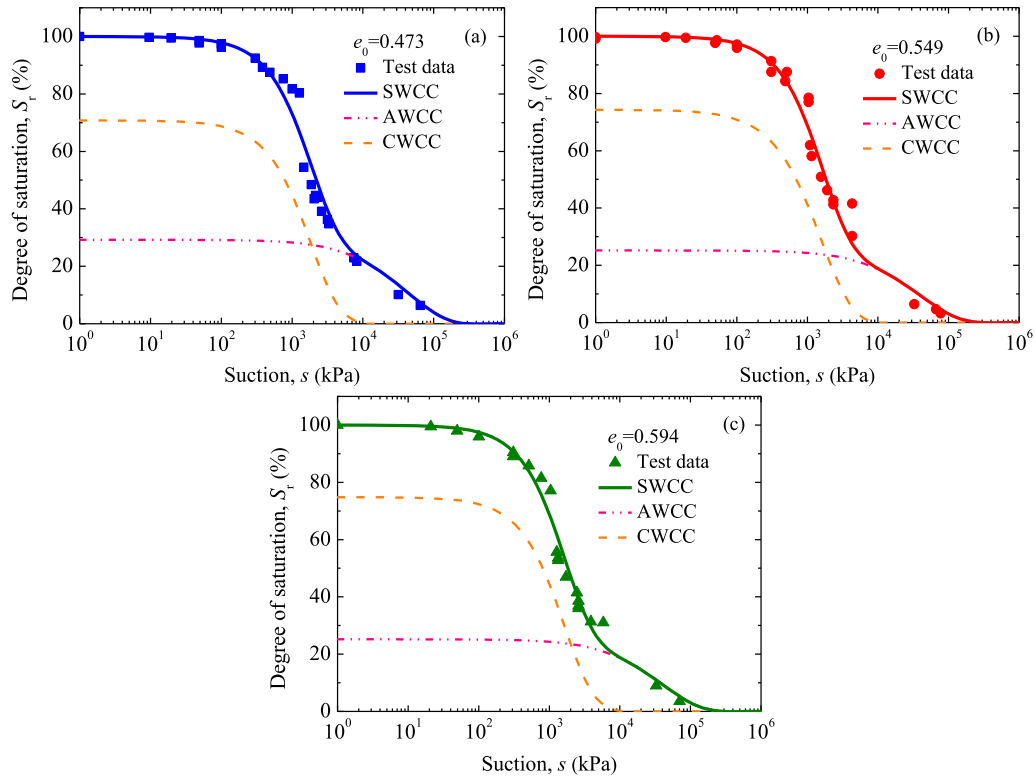


Fig. 8 Comparison of measured and fitted SWCCs of JF residual clay with **a** $e_0 = 0.473$, **b** $e_0 = 0.549$ and **c** $e_0 = 0.594$ (data from [7])

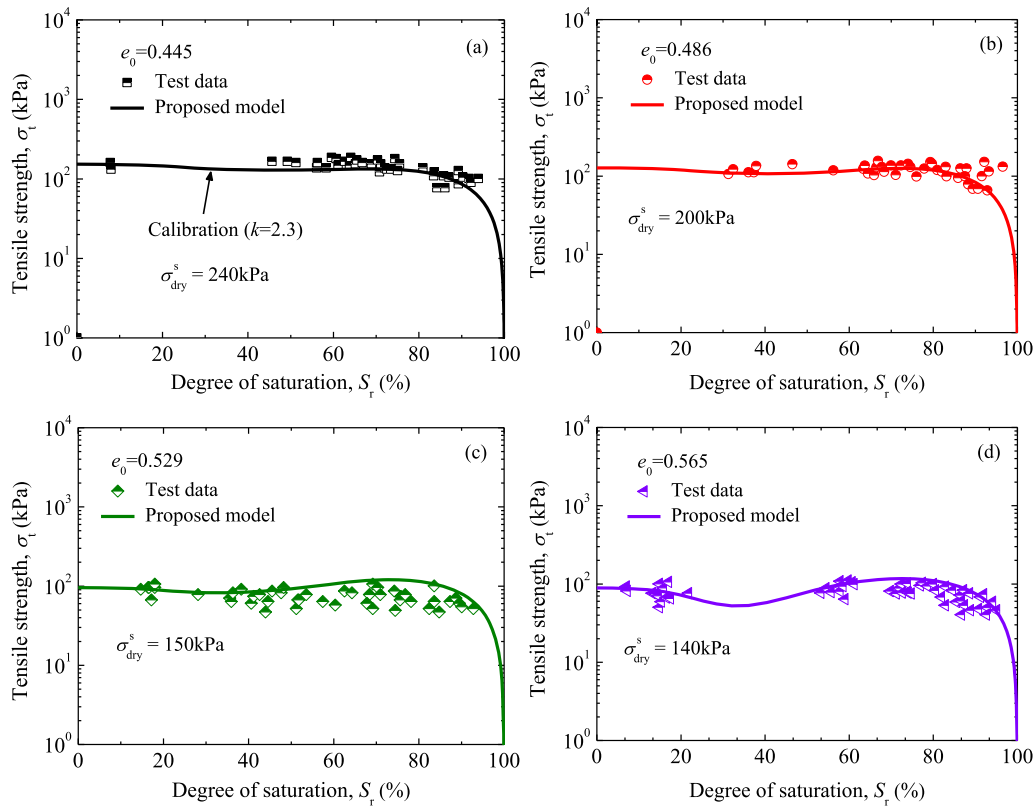


Fig. 9 Experimental validation of tensile strength model for BTG residual clay with **a** $e_0 = 0.445$, **b** $e_0 = 0.486$, **c** $e_0 = 0.529$ and **d** $e_0 = 0.565$ (data from [7])

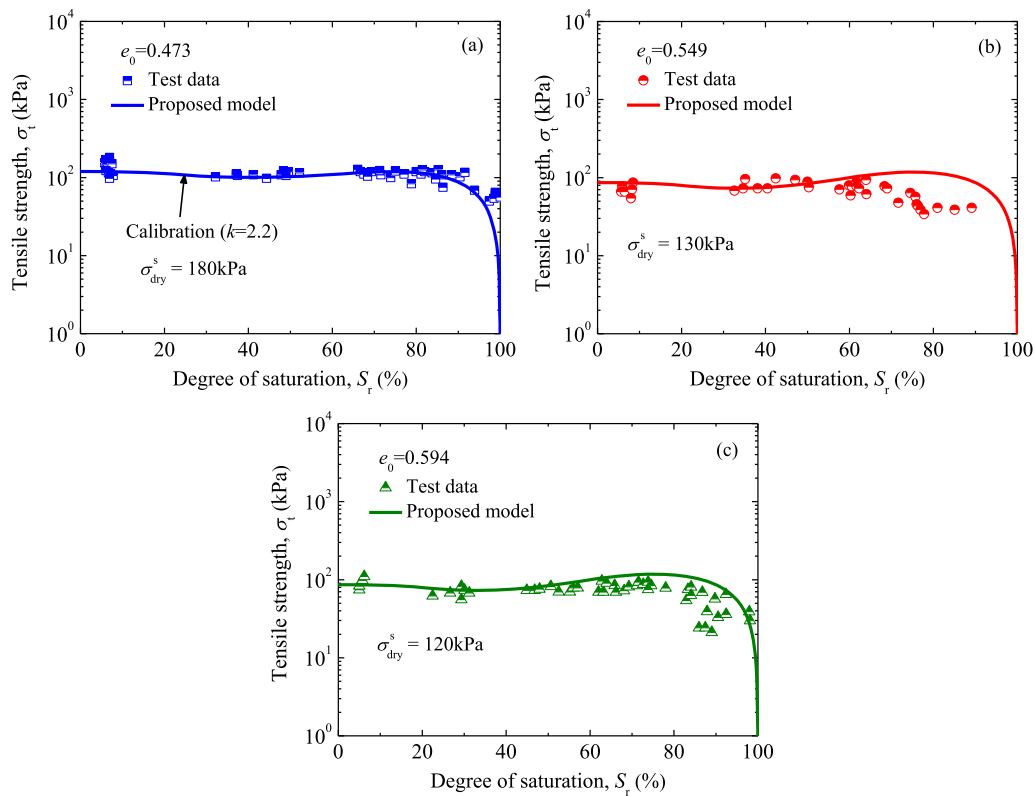


Fig. 10 Experimental validation of tensile strength model for JF residual soil with a $e_0 = 0.473$, b $e_0 = 0.549$ and c $e_0 = 0.594$ (data from [7])

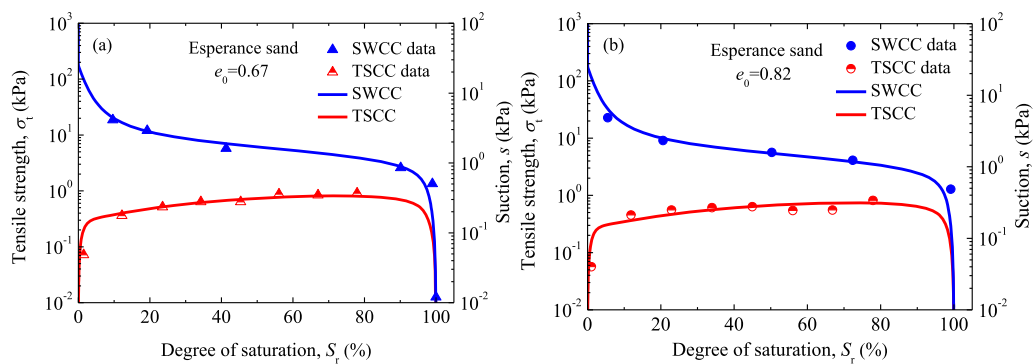


Fig. 11 Comparisons of the measured and predicted soil water retention curve, tensile strength characteristic curve for Esperance sand with a $e_0 = 0.67$ and b $e_0 = 0.82$ (data from Lu et al. [31])

Table 6 Parameters of proposed model for coarse-grained soils

| Soil name | b | s_r (kPa) | a | M | n |
|------------------|------|-------------|------|------|------|
| Esperance sand | 0.50 | 25 | 1.16 | 1.25 | 4.56 |
| Owatta sand | 0 | 100 | 3.20 | 2.50 | 2.40 |
| Perth silty sand | 0 | 200 | 3.52 | 2.30 | 2.15 |

0.82). The tensile strength of the Esperance sand at two constant porosity values was measured using a modified direct shear apparatus. The adopted model parameters for

Esperance sand are listed in Table 6, and an effective internal friction angle of 50° was used, yielding a good agreement.

Figure 12 shows model validation against measured data of two sand types (i.e. Ottawa sand and Perth sand). The complete test results for Ottawa sand and Perth sand were reported in Lu et al. [33] and Kim and Sture [23], respectively. The model parameters are presented in Table 6. The effective internal friction angles for Ottawa sand and Perth sand are 48° and 55° , respectively. An excellent agreement can be observed between the measured and predicted results of tensile strength for both sands.

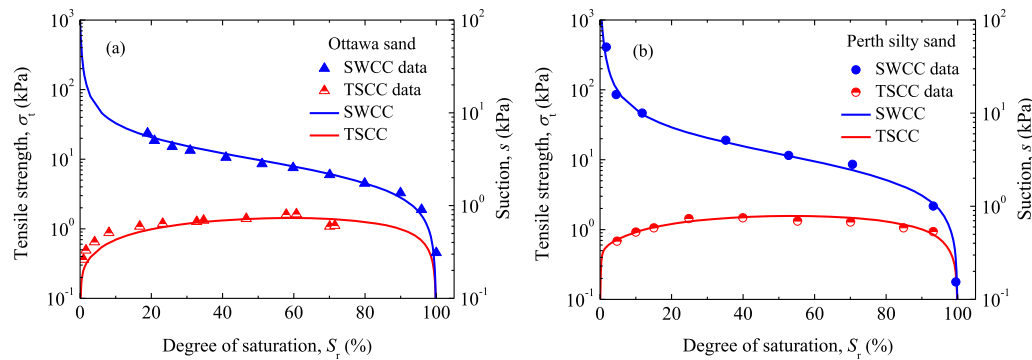


Fig. 12 Comparisons of the measured and predicted soil water retention curve, tensile strength characteristic curve for **a** Ottawa sand and **b** Perth silty sand

8 Conclusions

To investigate the behaviour of tensile strength of unsaturated soils, a series of tensile strength tests were firstly performed on compacted lean clays with different void ratios. Based on the observed phenomenon, a predictive model accounting for the tensile strength with different initial void ratios was developed based on the interaction mechanism between capillary water and adsorbed water. The conclusions can be summarized as follows:

1. The experimental results indicate that the tensile strength depends significantly on the initial water content at a given void ratio. The tensile strength of specimens with different void ratios first increased and then decreased with increasing water content, and a peak value of the tensile strength was observed at the critical water content.
2. A modified SWCC model accounting for the effect of initial void ratio was developed based on the interaction mechanism between capillary water and adsorbed water, which is shown to be able to accurately capture the soil water behaviour with different void ratios over a wide suction range.
3. Tensile strength model considering the effect of initial void ratio was established for both coarse-grained and fine-grained unsaturated soils. The proposed tensile strength models were verified by comparing against experimental results obtained in this study and those reported in the literature, showing an excellent agreement.

Acknowledgements The authors express their gratitude for the grants provided by the National Natural Science Foundation of China (Nos. 42272312, 52238007 and 41902279), the Fundamental Research Funds for the Provincial Universities of Zhejiang (SJLY2022007),

and Guangxi Key Laboratory of Geomechanics and Geotechnical Engineering (20YKF06).

References

1. ASTM D2487-11 (2006) Standard practice for classification of soils for engineering purposes (unified soil classification system). ASTM International, West Conshohocken
2. Akin ID, Likos WJ (2017) Brazilian tensile strength testing of compacted clay. *Geotech Test J* 40(4):608–617. <https://doi.org/10.1520/GTJ20160180>
3. Baker R, Frydman S (2009) Unsaturated soil mechanics: critical review of physical foundations. *Eng Geol* 106(1–2):26–39. <https://doi.org/10.1016/j.enggeo.2009.02.010>
4. Bao YD, Li YC, Zhang YS, Yan JH, Zhou X, Zhang XD (2022) Investigation of the role of crown crack in cohesive soil slope and its effect on slope stability based on the extended finite element method. *Nat Hazards* 110:295–314. <https://doi.org/10.1007/s11069-021-04947-8>
5. Beckett CTS, Smith JC, Ciancio D, Augarde CE (2015) Tensile strengths of flocculated compacted unsaturated soils. *Geotech Lett* 5(4):254–260. <https://doi.org/10.1680/jgele.15.00087>
6. Birle E, Heyer D, Vogt N (2008) Influence of the initial water content and dry density on the soil-water retention curve and the shrinkage behavior of a compacted clay. *Acta Geotech* 3(3):191–200. <https://doi.org/10.1007/s11440-008-0059-y>
7. Bulolo S, Leong EC, Kizza R (2021) Tensile strength of unsaturated coarse and fine-grained soils. *B Eng Geol Environ* 80(3):2727–2750. <https://doi.org/10.1007/s10064-020-02073-6>
8. Cai GQ, Shi PX, Kong XA, Zhao CG, Likos W (2020) Experimental study on tensile strength of unsaturated fine sands. *Acta Geotech* 15(5):1057–1106. <https://doi.org/10.1007/s11440-019-00807-9>
9. Cai GQ, Zhou AN, Liu Y, Xu RZ, Zhao CG (2020) Soil water retention behavior and microstructure evolution of lateritic soil in the suction range of 0–286.7 MPa. *Acta Geotech* 15(1):3327–3341. <https://doi.org/10.1007/s11440-020-01011-w>
10. Chen B, Peng F, Zhang L, Sun DA (2023) Investigation on swelling characteristics of GMZ bentonite with different initial water contents. *Ann Nucl Energy* 181:109565. <https://doi.org/10.1016/j.anucene.2022.109565>

11. Das BM, Yen SC, Dass RN (2015) Brazilian tensile strength test of lightly cemented sand. *Can Geotech J* 32(1):166–171
12. Fredlund DG, Rahardjo H (1993) *Soil mechanics for unsaturated soils*. Wiley, New York
13. Fredlund DG, Xing A (1994) Equation for the soil-water characteristic curve. *Can Geotech J* 31(4):521–532
14. Gallipoli D (2012) A hysteretic soil-water retention model accounting for cyclic variations of suction and void ratio. *Geotechnique* 62(7):605–616. <https://doi.org/10.1680/geot.11.P.007>
15. Gallipoli D, Wheeler SJ, Karstunen M (2003) Modelling the variation of degree of saturation in a deformable unsaturated soil. *Geotechnique* 53(1):105–112. <https://doi.org/10.1680/geot.2003.53.1.105>
16. Gao Y, Li Z, Sun DA, Yu HH (2021) A simple method for predicting the hydraulic properties of unsaturated soils with different void ratios. *Soil Till Res* 209:104913. <https://doi.org/10.1016/j.still.2020.104913>
17. Gao Y, Sun DA (2017) Soil-water retention behavior of compacted soil with different densities over a wide suction range and its prediction. *Comput Geotech* 91:17–26. <https://doi.org/10.1016/j.compgeo.2017.06.016>
18. Gao Y, Sun DA, Zhou AN, Li J (2020) Predicting shear strength of unsaturated soils over wide suction range. *Int J Geomech* 20(2):04019175. [https://doi.org/10.1061/\(ASCE\)GM.1943-5622.0001555](https://doi.org/10.1061/(ASCE)GM.1943-5622.0001555)
19. Gao Y, Sun DA, Zhu ZC, Xu YF (2019) Hydromechanical behavior of unsaturated soil with different initial densities over a wide suction range. *Acta Geotech* 14(2):417–428. <https://doi.org/10.1007/s11440-018-0662-5>
20. Khlosi M, Cornelis WM, Douaïk A, Van Genuchten MT, Gabriels D (2008) Performance evaluation of models that describe the soil water retention curve between saturation and oven dryness. *Vadose Zone J* 7(1):87–96. <https://doi.org/10.2136/vzj20070099>
21. Kim TH, Hwang C (2003) Modeling of tensile strength on moist granular earth material at low water content. *Eng Geol* 69(3–4):233–244. [https://doi.org/10.1016/S0013-7952\(02\)00284-3](https://doi.org/10.1016/S0013-7952(02)00284-3)
22. Kim TH, Kang GC, Ge L (2012) Factors influencing crack-induced tensile strength of compacted soil. *J Mater Civ Eng* 24(3):315–320. [https://doi.org/10.1061/\(ASCE\)MT.1943-5533.0000380](https://doi.org/10.1061/(ASCE)MT.1943-5533.0000380)
23. Kim TH, Sture S (2008) Capillary-induced tensile strength in unsaturated sands. *Can Geotech J* 45(5):726–737. <https://doi.org/10.1139/T08-017>
24. Konrad JM, Lebeau M (2015) Capillary-based effective stress formulation for predicting shear strength of unsaturated soils. *Can Geotech J* 52(12):2067–2076. <https://doi.org/10.1139/cgj-2014-0300>
25. Lee IM, Sung SG, Cho GC (2005) Effect of stress state on the unsaturated shear strength of a weathered granite. *Can Geotech J* 42(2):624–631. <https://doi.org/10.1139/t04-091>
26. Li HD, Tang CS, Cheng Q, Li SJ, Gong XP, Shi B (2019) Tensile strength of clayey soil and the strain analysis based on image processing techniques. *Eng Geol* 253(10):137–148. <https://doi.org/10.1016/j.enggeo.2019.03.017>
27. Liang QG, Wu XY, Li CQ, Wang LL (2014) Mechanical analysis using the unconfined penetration test on the tensile strength of Q3 loess around Lanzhou City, China. *Eng Geol* 183(9):324–329. <https://doi.org/10.1016/j.enggeo.2014.10.016>
28. Lu N (2016) Generalized soil water retention equation for adsorption and capillarity. *J Geotech Geoenviron Eng* 142(10):04016051. [https://doi.org/10.1061/\(ASCE\)GT.1943-5606.0001524](https://doi.org/10.1061/(ASCE)GT.1943-5606.0001524)
29. Lu N, Godt JW, Wu DT (2010) A closed-form equation for effective stress in unsaturated soil. *Water Resour Res* 46(5):W05515. <https://doi.org/10.1029/2009WR008646>
30. Lu N, Khorshidi M (2015) Mechanism for soil-water retention and hysteresis at high suction range. *J Geotech Geoenviron Eng* 141(8):04015032. [https://doi.org/10.1061/\(ASCE\)GT.1943-5606.0001325](https://doi.org/10.1061/(ASCE)GT.1943-5606.0001325)
31. Lu N, Kim TH, Sture S, Likos WJ (2009) Tensile strength of unsaturated sand. *J Eng Mech* 135(12):1410–1419. [https://doi.org/10.1061/\(ASCE\)EM.1943-7889.0000054](https://doi.org/10.1061/(ASCE)EM.1943-7889.0000054)
32. Lu N, Likos WJ (2006) Suction stress characteristic curve for unsaturated soil. *J Geotech Geoenviron Eng* 132(2):131–142. [https://doi.org/10.1061/\(ASCE\)1090-0241\(2006\)132:2\(131\)](https://doi.org/10.1061/(ASCE)1090-0241(2006)132:2(131))
33. Lu N, Wu BL, Tan CP (2007) Tensile strength characteristics of unsaturated sands. *J Geotech Geoenviron Eng* 133(2):144–154. [https://doi.org/10.1061/\(ASCE\)1090-0241\(2007\)133:2\(144\)](https://doi.org/10.1061/(ASCE)1090-0241(2007)133:2(144))
34. Narvaez B, Aubertin M, Saleh-Mbemba F (2015) Determination of the tensile strength of unsaturated tailings using bending tests. *Can Geotech J* 52(11):1874–1885. <https://doi.org/10.1139/cgj-2014-0156>
35. Revil A, Lu N (2013) Unified water isotherms for clayey porous materials. *Water Resour Res* 49(9):5685–5699. <https://doi.org/10.1139/cgj-2015-0322>
36. Romero E, Gens A, Lloret A (1999) Water permeability, water retention and microstructure of unsaturated compacted Boom clay. *Eng Geol* 54(1–2):117–127. [https://doi.org/10.1016/S0013-7952\(99\)00067-8](https://doi.org/10.1016/S0013-7952(99)00067-8)
37. Salimi K, Cerato A, Vahedifard F, Miller GA (2021) General model for the uniaxial tensile strength characteristic curve of unsaturated soils. *J Geotech Geoenviron Eng* 147(7):04021051. [https://doi.org/10.1061/\(ASCE\)GT.1943-5606.0002567](https://doi.org/10.1061/(ASCE)GT.1943-5606.0002567)
38. Tamrakar SB, Mitachi T, Toyosawa Y (2007) Measurement of soil tensile strength and factors affecting its measurements. *Soils Found* 47(5):911–918. <https://doi.org/10.3208/sandf.47.911>
39. Tang CS, Pei XJ, Wang DY, Shi B, Li J (2015) Tensile strength of compacted clayey soil. *J Geotech Geoenviron Eng* 141(4):04014122. [https://doi.org/10.1061/\(ASCE\)GT.1943-5606.0001267](https://doi.org/10.1061/(ASCE)GT.1943-5606.0001267)
40. Tang LS, Zhao ZL, Luo ZG, Sun YL (2019) What is the role of tensile cracks in cohesive slopes? *J Rock Mech Geotech* 11(2):314–324. <https://doi.org/10.1016/j.jrmge.2018.09.007>
41. Trabelsi H, Romero E, Jamei M (2018) Tensile strength during drying of remoulded and compacted clay: the role of fabric and water retention. *Appl Clay Sci* 162(15):57–68. <https://doi.org/10.1016/j.clay.2018.05.032>
42. Tran KQ, Satomi T, Takahashi H (2019) Tensile behaviors of natural fiber and cement reinforced soil subjected to direct tensile test. *J Build Eng* 24:100748. <https://doi.org/10.1016/j.jobe.2019.100748>
43. Varsei M, Miller GA, Hassanikah A (2016) Novel approach to measuring tensile strength of compacted clayey soil during desiccation. *Int J Geomech* 16(6):D4016011. [https://doi.org/10.1061/\(ASCE\)GM.1943-5622.0000705](https://doi.org/10.1061/(ASCE)GM.1943-5622.0000705)
44. Wang JP, François B, Lambert P (2020) From basic particle gradation parameters to water retention curves and tensile strength of unsaturated granular soils. *Int J Geomech* 26(6):1–10. [https://doi.org/10.1061/\(ASCE\)GM.1943-5622.0001677](https://doi.org/10.1061/(ASCE)GM.1943-5622.0001677)
45. Yin PH, Vanapalli SK (2018) Model for predicting tensile strength of unsaturated cohesionless soils. *Can Geotech J* 55(9):1313–1333. <https://doi.org/10.1139/cgj-2017-0376>

46. Zhai Q, Rahardjo H, Satyanaga A, Dai GL (2020) Estimation of tensile strength of sandy soil from soil-water characteristic curve. *Acta Geotech* 15(12):3371–3381. <https://doi.org/10.1007/s11440-020-01013-8>
47. Zhang C, Lu N (2020) Unified effective stress equation for soil. *J Eng Mech* 146(2):04019135. [https://doi.org/10.1061/\(ASCE\)EM.1943-7889.0001718](https://doi.org/10.1061/(ASCE)EM.1943-7889.0001718)
48. Zhang JR, Niu G, Li XC, Sun DA (2020) Hydro-mechanical behavior of expansive soils with different dry densities over a wide suction range. *Acta Geotech* 15(1):265–278. <https://doi.org/10.1007/s11440-019-00874-y>
49. Zhou AN, Huang RQ, Sheng DC (2016) Capillary water retention curve and shear strength of unsaturated soils. *Can Geotech J* 141(8):04015032. <https://doi.org/10.1139/cgj-2015-0322>

Publisher's Note Springer Nature remains neutral with regard to jurisdictional claims in published maps and institutional affiliations.